Biophysical Journal Volume 105 October 2013 1822–1828

IR Laser-Induced Perturbations of the Voltage-Dependent Solute Carrier Protein SLC26a5

Oluwarotimi Okunade[†] and Joseph Santos-Sacchi[†‡§*]

[†]Department of Surgery (Otolaryngology), [‡]Department of Neurobiology, and [§]Department of Cellular and Molecular Physiology, Yale University School of Medicine, New Haven, Connecticut

ABSTRACT Alterations in membrane capacitance can arise from linear and nonlinear sources. For example, changes in membrane surface area or dielectric properties can modify capacitance linearly, whereas sensor residues of voltage-dependent proteins can modify capacitance nonlinearly. Here, we examined the effects of fast temperature jumps induced by an infrared (IR) laser in control and prestin (SLC26a5)-transfected human embryonic kidney (HEK) cells under whole-cell voltage clamp. Prestin's voltage sensor imparts a characteristic bell-shaped, voltage-dependent nonlinear capacitance (NLC). Temperature jumps in control HEK cells cause a monophasic increase in membrane capacitance (C_m) regardless of holding voltage due to double-layer effects. Prestin-transfected HEK cells, however, additionally show a biphasic increase/decrease in C_m with a reversal potential corresponding to the voltage at peak NLC of prestin (V_h), attributable to a rapid temperature-following shift in V_h, with shift rates up to 14 V/s over the course of a 5 ms IR pulse. Treatment with salicylate, a known inhibitor of NLC, reestablishes control cell behavior. A simple kinetic model recapitulates our biophysical observations. These results verify a voltage-dependent protein's ability to respond to fast temperature perturbations on a par with double-layer susceptibility. This likely arises from prestin's unique ability to move sensor charge at kilohertz rates, which is required for the outer hair cells' role as a cochlear amplifier.

INTRODUCTION

Outer hair cells (OHCs) are mechanically active components of the inner ear that underlie cochlear amplification (1). Cochlear amplification denotes a process whereby responses to low-level acoustic stimuli are enhanced, resulting in an increase in auditory sensitivity and frequency-resolving power. This is accomplished by OHCs feeding back mechanical energy into the vibrating sensory organ to boost stimulation to the inner hair cells, which are predominantly innervated by the auditory nerve. Prestin motor units (SLC26a5), proteins of the SLC26 anion transporter family (2), are localized to the OHC lateral membrane, drive rapid mechanical changes in OHCs, and are associated with nonlinear capacitance (NLC). NLC arises as the first derivative of a two-state Boltzmann function relating prestin voltage-sensor charge as a function of transmembrane voltage. It reflects the movement of charged residues within these motor units and peaks at a voltage (V_h) to which the OHCs' mechanical response is maximally sensitive. NLC is vulnerable to biophysical forces, including temperature and membrane tension (3–8).

Here, we examine the effects of fast temperature jumps induced by an infrared (IR) laser in control and prestin-transfected human embryonic kidney (HEK) cells under whole-cell voltage clamp. We find effects on both linear and prestin-derived NLC. Whereas fast temperature jumps monotonically increase linear C_m in a voltage-independent manner, the Boltzmann distribution of motors along the voltage axis is rapidly and simultaneously altered in a reversible manner. Our observations clearly show that voltage-dependent proteins, given sufficiently fast kinetics (as with prestin), can contribute to rapid alterations of membrane capacitance.

MATERIALS AND METHODS

Cell culture and expression

We previously developed a tetracycline-inducible HEK293 cell line that highly expresses prestin (9). Here, we cultured HEK293 cells in Dulbecco's modified Eagle's high glucose base medium (DMEM) containing 50 U/ml each of penicillin, streptomycin, and L-glutamine, supplemented with 10% fetal bovine serum, 5 μg/ml of blasticidin, and 130 μg/ml of zeocin. The cells were maintained at 37°C in a humidified incubator gassed with 5% CO_2. The addition of 1 microgram/ml tetracycline to the growth medium induced prestin expression and trafficking to the cell membrane. Patch-clamp recordings of the cells were made 24–72 hr after induction at room temperature.

IR laser

Photonic stimulation with a Capella R-1850 laser was used to deliver rapid temperature jumps to cells in the recording chamber. The laser was coupled to a 600-μm-diameter optical fiber that delivered an output wavelength of 1850 nm in pulses of variable duration. At a power setting of 100%, the optical pulse energy was 5 mJ/ms. Laser stimulation was computer-controlled via TTL and synchronized to voltage clamp commands using an Axon Instruments 1320 series A/D and D/A board. The laser fiber was mounted on a micromanipulator and the tip was placed within 0.5 mm of the recorded cell, ensuring that the whole cell was irradiated.

Submitted June 18, 2013, and accepted for publication September 10, 2013.

*Correspondence: joseph.santos-sacchi@yale.edu

Editor: Joseph Mindell.

0006-3495/13/10/1822/7 $2.00

http://dx.doi.org/10.1016/j.bpj.2013.09.008

We assume that our observations arise from temperature changes within the membrane fostered by temperature changes in bath solution water, in accord with conclusions made in previous studies (10,11). We calibrated the temperature change indirectly by monitoring changes in patch electrode resistance (R_s, i.e., changes in I_{Rs} with fixed voltage stimulation) as in the previous studies. Thus, in preliminary experiments, we correlated R_s versus changes in whole bath temperature. In the physiological experiments, our admittance analysis of currents allowed us to quantify R_s changes independently of C_m and R_m changes (12). We found that a 33% change in R_s indicated a temperature change of 17°C. In our experiment, peak R_s change averaged 31.2 ± 0.02% ($n = 5$) at 40% laser power. Our previous observation that a 20 mV shift in NLC V_h occurs per 10°C change in bath temperature corroborates these estimates (3,4).

Patch-clamp electrophysiology

Ionic blocking solutions were used to remove voltage-dependent ionic conductances so that capacitive currents could be analyzed in isolation. Extracellular bath solutions for whole-cell recording in HEK293 cells consisted of (mM) 20 TEA, 20 CsCl, 2 $CoCl_2$, 1 $MgCl_2$, 10 Hepes, 1 $CaCl_2$, 100 NaCl adjusted to pH 7.22 with NaOH, and 301 mOsm using D-glucose. An extracellular perfusion solution containing 132 NaCl, 2 $CaCl_2$, 2 $MgCl_2$, 10 Hepes, 10 Na salicylate (pH 7.20, 300 mOsm) was also used for experiments to block NLC. Electrodes were filled with (mM) 140 CsCl, 2 $MgCl_2$, 10 Hepes, 10 EGTA (pH 7.27, 302 mOsm). All chemicals used were purchased from Sigma.

Borosilicate glass pipettes were pulled using a P-2000 laser-heating pipette puller (Sutter Instruments) to initial resistances ranging between 3.5 and 5 MΩ. Pipette stray capacitance was compensated for before recordings were obtained, and voltages were corrected for effects of series resistance offline. A Nikon Eclipse TE300 inverted microscope with Hoffmann optics was used to observe the cells during electrical recording. Round, isolated cells growing on a glass coverslip were patched 24–72 hr after tetracycline induction.

Cells were clamped to a holding potential of 0 mV using an Axon 200B patch-clamp amplifier. During the temperature jump protocol, cells were held under voltage clamp at 0 mV and stepped in 30 mV increments (from hyperpolarizing values of −150 mV to 150 mV) for 1024 ms during which a brief IR laser pulse was delivered to the cells for each voltage step. Solution exchange (e.g., with salicylate) was performed using gravity flow. All recordings were made at room temperature. Local temperature measurements of the cells were calculated by measuring changes in electrode resistance and extrapolating from a resistance-temperature calibration curve (11). A resistance-temperature calibration curve was obtained by observing changes in pipette resistance in a hot bath solution (~55°C) that was allowed to cool passively.

Cell capacitance was measured under a whole-cell configuration using jClamp software (SciSoft, CT; www.SciSoftCo.com). Voltage records sampled at 10 μs were filtered at 10 kHz with an eight-pole Bessel filter and saved to disk for offline analysis. NLC was measured using a continuous high-resolution (2.56 ms sampling), two-sine stimulus protocol (10 mV peak at both 390.6 and 781.2 Hz) superimposed onto the voltage command (12,13). Capacitance data were fit to the first derivative of a two-state Boltzmann function (14):

$$C_m = Q_{\max}\frac{ze}{kT}\frac{b}{(1+b)^2} + C_{lin},\; b = \exp\left(\frac{-ze(V_m - V_h)}{kT}\right) \quad (1)$$

where Q_{max} is the maximum nonlinear charge moved; V_h is voltage at peak capacitance or, equivalently, at half-maximum charge transfer; V_m is membrane potential; z is valence; C_{lin} is linear membrane capacitance; e is electron charge; k is Boltzmann's constant; and T is absolute temperature. Our justification for using steady-state fits of prestin's charge movement at the 2.56 ms C_m measurement sampling rate is that the parameters are largely stable (z, Q_{max}), except for V_h, across time samples. ΔC_m is defined as the difference between pre-IR and post-IR maximal capacitance. Results are reported as the mean ± standard error (SE).

Model

To understand the biophysical data, we used a kinetic model of SLC26a5 that we previously developed (15). The model was developed to account for a chloride-dependent disparity between NLC and electromotility V_h, requiring intermediate transitions much slower than either chloride- or voltage-dependent transitions. A model cartoon is shown in Fig. 5 *A* of Song and Santos-Sacchi (15).

$$X_o \underset{k_2}{\overset{k_1}{\rightleftharpoons}} X_c \underset{\beta_0}{\overset{\alpha_0}{\rightleftharpoons}} X \underset{\beta}{\overset{\alpha}{\rightleftharpoons}} C \quad (2)$$

State X_o is SLC26a5 in the absence of bound anion; state X_c is with bound anion; state X is voltage-enabled after anion binding, with its residence being favored by hyperpolarization (expanded state); and state C results from depolarization (contracted state). The model has very fast anion (chloride) binding and unbinding transitions ($X_o \leftrightarrow X_c$) and very fast voltage-dependent conformational transitions ($X \leftrightarrow C$). The transition to state $\boldsymbol{C}$ carries a unit charge, q; Q_{max}, the total charge moved, will reflect the maximal accumulation of motors in that state. Nestled between the anion-binding and voltage-dependent transitions resides a nonvoltage-dependent transition ($X_c \leftrightarrow X$), which is very much slower than the other two transitions.

We assessed the kinetic model using MATLAB (The MathWorks, Natick, MA) Simulink via an automation link with jClamp (www.scisoftco.com). The kinetic model was interfaced to jClamp via a model of the patch-clamp amplifier and cell. The linear component of the patch-cell model possessed an R_s of 5 MΩ, R_m of 500 MΩ, and C_{lin} of 10 pF. The nonlinear component, NLC, derived from charge movement of the SLC26a5 model, with the following parameters: $k_1 = 10^7 * [Cl]_{in}$, $k_2 = 10^7 * k_d$, $\alpha_0 = 75 * \exp(t_m)$, $\beta_0 = 95$, $\alpha = 10^6 * \exp(zFV_m/2RT)$, $\beta = 583 * 10^9 * \exp(-zFV_m/2RT + t_m/2 - E_a/RT)$, $k_{d\,Cl} = 0.001$, $T = 296$ kelvin, $E_a = 45$ kJ/mol, F = $9.648 * 10^4$ C/mol, $R = 8.315$ *J*/Kmol, $k = 1.381 * 10^{-23}$ VC/K.

The rates α_0 and β are tension sensitive because tension is known to increase prestin residence in the expanded (X) state (5,6), t_m in units kT (eRT/F); the rate β is temperature sensitive, with Arrhenius activation energy, E_a. α and β are voltage dependent, with sensor valence $z = 0.7$. At $T = 296$ K, $V_m = 0$ mV, $T_m = 0$ kT, and $[Cl]_{in} = 0.14$ M, initial rates are $k_1 = 1.4e6$, $k_2 = 1e4$, $\alpha_0 = 75$, $\beta_0 = 95$, $\alpha = 1e6$, and $\beta = 1e5$. Chloride concentrations and K_d are in molar; rates are $1/t$, with time (t) being 1 s. Voltage is in volts.

RESULTS

Capacitance

The rapid temperature change associated with an IR laser pulse delivered directly to a cell via optical fiber alters membrane capacitance. Control HEK cells and cells of our uninduced SLC26a5 HEK cell line increase their linear membrane capacitance in a voltage-independent fashion. Fig. 1 *A* shows C_m measures of a voltage-clamped, uninduced SLC26a5 HEK cell for a wide range of holding potentials. The delivery of a 20 ms IR pulse (40% of maximal laser power) induces a linearly ramped increase in C_m coinciding with the duration of the pulse. To better visualize the overlapped traces and indicate holding voltage, we offset the

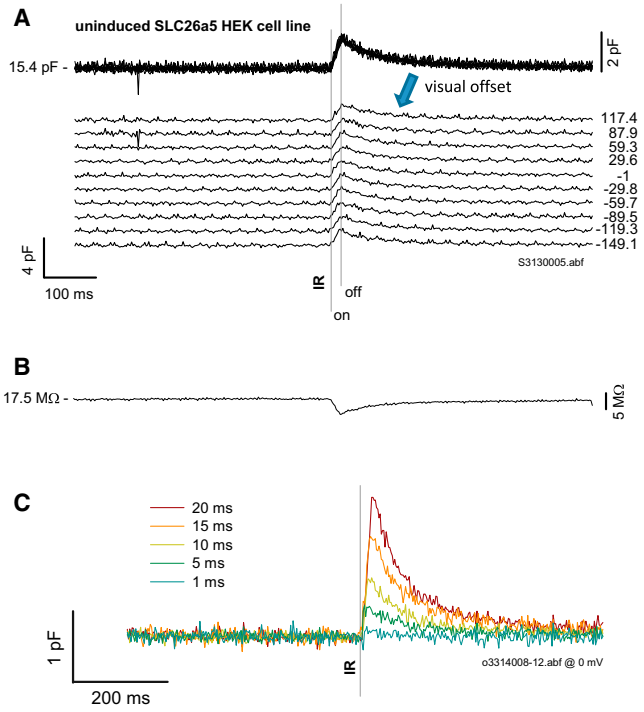

FIGURE 1 IR laser-induced temperature jump alters linear capacitance. (*A*) Under whole-cell voltage clamp, an uninduced SLC26a5 HEK cell was nominally stepped to the membrane potentials indicated. During the voltage step, an IR laser pulse of 20 ms duration (nominally 40% Capella laser power) was delivered via optical fiber. Regardless of the holding potential, the laser pulse induced a fixed maximal increase in C_m, ~10% of resting C_m. Averages are given in Results section. (*B*) Simultaneously measured series resistance indicates a linear increase in temperature during the pulse and an exponential cooling of bath media after the pulse. (*C*) An increase in duration of the pulse results in a greater C_m change. The holding potential is 0 mV.

traces by an arbitrary constant, allowing clearer observation of the voltage independence. The increase in C_m is 10.8% ± 2.5% ($n = 5$) of whole-cell capacitance for a 20 ms pulse. In Fig. 1 *A*, at laser offset, a single exponential decrease in C_m occurs with a time constant of 70 ms at 0 holding potential (81.5 ± 3.2 ms; $n = 5$). These linear and exponential phases of C_m change correspond, respectively, to a linear increase in temperature during the pulse and an exponential cooling of the bath solution/cytoplasm after the pulse, both of which are reflected in simultaneous changes in the series resistance of the pipette electrode (Fig. 1 *B*). Our admittance analysis allows us to quantify R_s changes, which are known to correspond to temperature manipulations (11). Fig. 1 *C* shows that increases in pulse durations induce increasing temperature changes that evoke larger C_m responses. Within our exposure range, we do not see any threshold effect for cell damage that is not associated with loss of cell recording.

In our SLC26a5 HEK cell line after tetracycline induction, cells possess a voltage-dependent NLC atop their linear capacitance (16). This arises from the voltage sensor activity underlying the protein's role in OHC electromotility (3,4).

Fig. 2 illustrates the voltage-dependent nature of the induced HEK cell's C_m, and the influence of temperature jumps on NLC and linear C_m. Again, we offset the overlapped traces by an arbitrary constant, allowing clearer observation of the effects of IR pulse on C_m; obvious differences are found in comparison with uninduced HEK cells (see Fig. 1). Indeed, a voltage-dependent effect is now observed. In Fig. 2 *B*, C_m-V_m functions are plotted at various time points relative to the start of the IR pulse. The laser pulse induced a shift of the C_m-V_m relation in the depolarizing direction. After correction of voltages for R_s effects, Boltzmann fits to the data (see Materials and Methods) allow a high-resolution (2.56 ms) inspection of dynamic changes in NLC and linear capacitance during and after the IR pulse (Fig. 2 *C*). In this example, NLC V_h shifted 40 mV in 20 ms at a linear rate of 2.03 V/s (average is 2.32 ± 0.21 V/s; $n = 6$) during the heating phase, and recovers (with temperature) exponentially with a time constant of 73 ms (average is 65.4 ± 10.8 ms; $n = 6$) during the cooling phase. The shift in V_h represents a redistribution of prestin motors into the

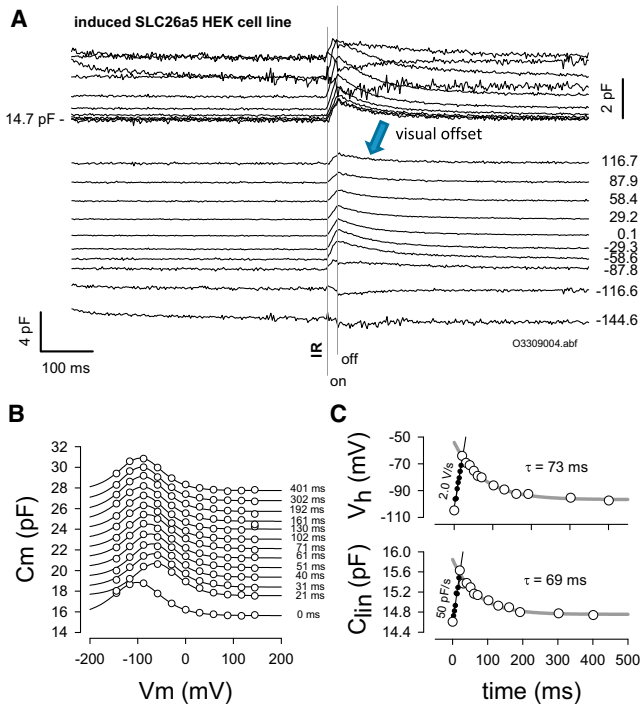

FIGURE 2 IR laser-induced temperature jump alters SLC26a5-generated NLC and linear capacitance. (*A*) Under whole-cell voltage clamp, an induced SLC26a5 HEK cell was nominally stepped to the membrane potentials indicated. During the voltage step, an IR laser pulse of 20 ms duration (nominally 40% Capella laser power) was delivered via optical fiber. The laser pulse induced a maximal change in C_m that depended on the holding potential. The change could be either an increase or decrease. (*B*) C_m-V_m plots of NLC as a function of time after pulse onset. Note the effect on the voltage dependence of NLC, namely, a shift to the right. (*C*) Changes in V_h and C_{lin} follow temperature. Rapid shifts and increases in C_{lin} occur during laser heating and return back to initial levels during bath cooling. Averages are given in the Results section. To see this figure in color, go online.

expanded conformation during heating. We previously observed this shift over the course of minutes using Peltier control of the bath solution temperature, with the shift averaging ~20 mV/10°C (3,4). In two additional cells, we were able to determine the V_h shift with 5 ms pulses at 90% laser power. The shift was 67 and 70 mV in 5 ms or 13.4 and 14 V/s, indicating that heating rates and corresponding V_h shift rates increase with greater laser power. The increase in rates with laser power indicates that we have yet to observe the fastest response and are limited by the laser power (for technical reasons, we avoid >90% power usage). Linear capacitance also changes simultaneously, with a time course similar to that of NLC V_h. In this case, there is a linear change of 50 pF/s during heating and a recovery due to cooling with a time constant of 69 ms (average is 78.9 ± 7.7 ms; $n = 6$). The changes due to cooling in linear capacitance are similar to those observed in control HEK cells. These rapid rates of change during heating and cooling mirror the changes in temperature as gauged from R_s inspection or predicted from previous observations on temperature-dependent shifts of V_h during slow bath changes in temperature (3,4), i.e., they correspond to a temperature-induced change of 20 mV/10°C.

The difference in susceptibility of NLC and linear C_m to temperature jump is readily illustrated by the behavior of ΔC_m, defined as the maximal difference between pre-IR and post-IR capacitance. Examples from two cells are shown in Fig. 3, *A* and *B*. Whereas IR pulse-induced linear C_m changes occur at the same magnitude and direction (increase) regardless of the holding potential (Fig. 1), NLC changes vary depending on the holding potential, and reverse in direction near voltages (average is −96.8 ± 6.4 mV; $n = 5$) around NLC V_h (average is −94.7 ± 6.2 mV; $n = 5$), with an R^2 value of 0.9943 (Fig. 3, *A* and *B*). Thus, it is possible, depending on the magnitude of NLC and its V_h (relative to holding potential), to induce a decrease in C_m by IR laser pulse. Salicylate (10 mM) not only reduces NLC, as expected (18,19), but also eliminates the characteristic reversal of ΔC_m normally afforded by SLC26a5 expression, essentially returning the induced HEK cell back to its preinduced condition ($n = 2$). That is, only an increase in C_m is observed, regardless of the holding potential (Fig. 3 *A*).

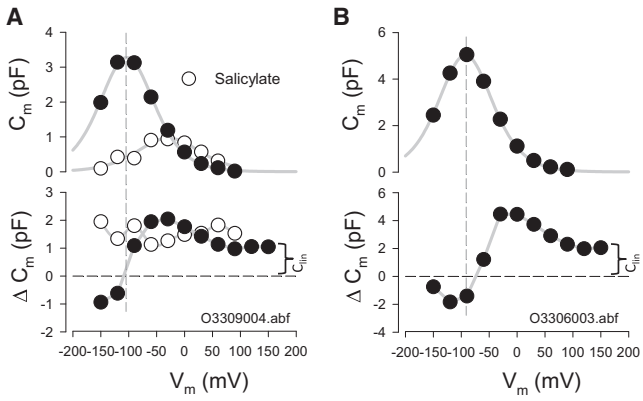

FIGURE 3 IR laser-induced temperature jump alters NLC showing increases and decreases that reverse near V_h of NLC. The NLC plotted is the one before the temperature jump. (*A* and *B*) Shown are data from two cells. ΔC_m at positive voltages remains offset from zero due to the temperature-dependent increase in linear C_m (*curly brackets*). In the first case (*A*), after data collection, salicylate (10 mM) was perfused onto the cell and collection was repeated. Salicylate removes the ΔC_m reversal as a result of NLC block, leaving intact a constant linear C_m increase across holding voltage. Averages are given in Results.

To understand the data, we evaluated the temperature-dependent behavior of a recently developed kinetic model of SLC26a5 (15). In this model (see Materials and Methods), only the backward, voltage-dependent transition, β, is temperature sensitive, indicating that only movements into the hyperpolarized (expanded) state of SCL26a5 are affected by temperature. In the simulation, we simply modeled the temperature change as that revealed by our experimental measures of R_s (in this case, with a 23°C maximum change; Fig. 4 *A*). Similar to the biophysical data, a rapid temperature change followed by cooling induced characteristic changes in C_m, which derived from NLC magnitude and induced V_h shifts (Fig. 4, *B* and *C*). As we deduced from the biophysical data, NLC V_h shifts directly mirror temperature changes. To match the average biophysical data of 2.3V/s (~20 mV/10°C), an Arrhenius activation energy of 45 k J/mol was required. The model also recapitulates the reversal of ΔC_m near V_h (Fig. 4 *D*). Also note that ΔC_m recovers with temperature back to zero at voltages away from V_h, in contrast to the biophysical data (Fig. 3), because the original model had no temperature-sensitive linear C_m (Fig. 4, *solid circles*). However, when a linearly temperature-dependent C_m is introduced, ΔC_m appears more similar to the biophysical data (Fig. 4 *D*, *open circles*). The original implementation of the kinetic model (15) had temperature dependence of both the backward intermediate rate, β_0, and the backward voltage-dependent rate, β. Here, however, we obtained better correspondence to the biophysical data by setting temperature dependence only in β.

Currents

We found two components of currents associated with fast temperature jump (Fig. 5). The first component coincided with the IR heating phase and its magnitude was related to the rate of heating (or correspondingly to the rate of linear C_m change; Fig. 5, *A* and *B*). This current appeared to reverse at positive voltages, as found by Shapiro et al. (10) (Fig. 5 *C*). We agree with their discussion on the matter, especially their interpretation that this may arise from asymmetrical fixed charges on the membrane leaflets. The second, slower component, which reversed near 0 mV, peaked at maximal temperature and then decayed during the cooling phase (Fig. 5, *C* and *D*). We interpret this as

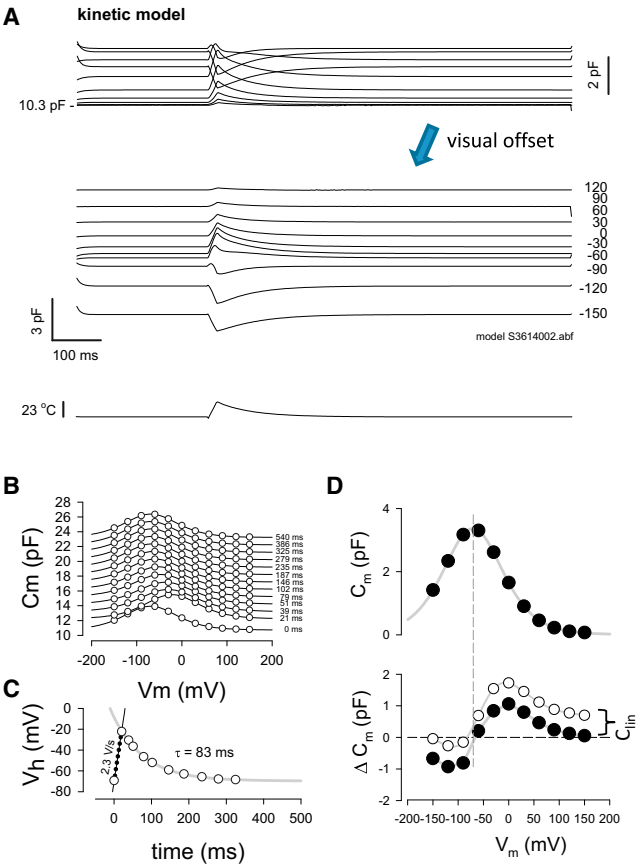

FIGURE 4 A kinetic model recapitulates biophysical data. (*A*) Stimulation with the experimentally observed temperature change induced by an IR laser pulse induces C_m behavior similar to the biophysical results. Here, the model transition rates are set to give a V_h of −71 mV. (*B*) Plots of NLC show rightward shifts along the voltage axis as a result of temperature increase. (*C*) Rates of V_h shift are comparable to biophysical data and directly follow temperature alterations. (*D*) Voltage at reversal of ΔC_m is related to V_h. Note that ΔC_m goes back to zero, in contrast to the biophysical data, when C_{lin} is not temperature sensitive (*closed circles*). Including temperature dependence for C_{lin} results in an offset similar to the biophysical data (*open circles*, *curly brackets*). To see this figure in color, go online.

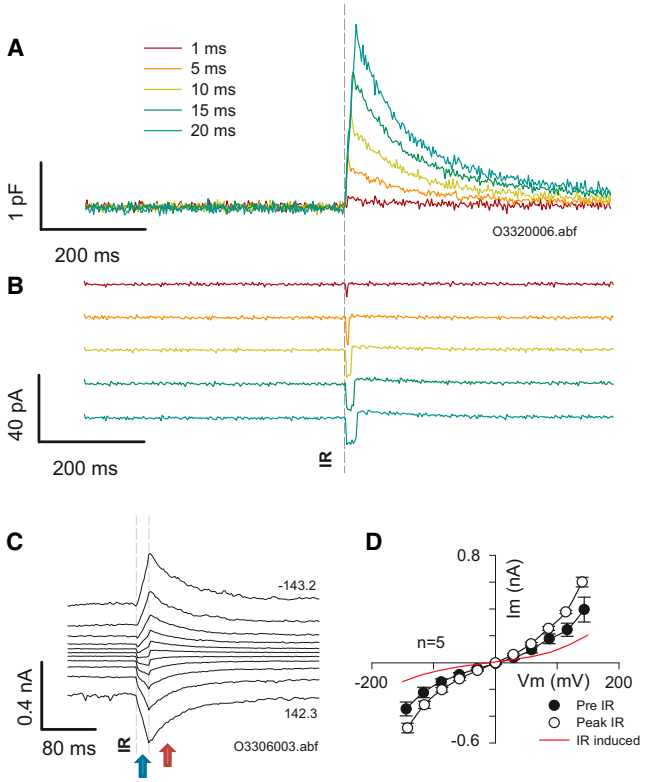

FIGURE 5 Two components of current induced during temperature jump. (*A* and *B*) Capacitance increases during temporally incremental IR laser pulses (*A*) and corresponding currents arise (*B*). Current magnitude depends on rate of C_m change and duration depends on pulse duration. For all traces, pulses were delivered at a holding potential of 0 mV. (*C*) Current responses for a 20 ms duration pulse within the holding potential extremes indicated, stepped nominally at 30 mV. Note the fast inward current response during the laser pulse, with a reversal potential predicted to be at positive potentials. Simultaneously, a slow-decaying current with reversal near 0 mV is observed. The red arrow shows the sum of the two components (note step behavior around zero potential that rides on the slower current ramp) and the blue arrow shows the slow component after the fast component ends after the laser pulse. (*D*) IV plot of average cell currents before and at termination of the IR pulse (mean ± SE; $n = 5$). The red line is IR-induced current. Note that current voltage dependence is unaffected by temperature, unlike that of NLC.

an ionic current that is nonspecific with a reversal potential near zero. Sometimes we found that the second, slower component obscured the first component as described in Shapiro et al. (10). Nevertheless, the rapid component is clearly observable in the traces near zero potential (Fig. 5 *C*). The second, slow-decaying membrane current displays nonlinear features (Fig. 5 *D*) reminiscent of G_{metL}, a conductance found in OHCs with marked temperature dependence (20,21). The current increase due to IR stimulation is likewise nonlinear, and therefore is unlikely due to linear decreases in R_s with temperature.

DISCUSSION

Control HEK cells and HEK cells expressing the voltage-dependent protein SLC26a5 show very fast changes in membrane capacitance when rapid temperature jumps are delivered to the cells by IR laser. For control cells, rapid alterations in linear C_m directly follow changes in temperature, as observed by Shapiro et al. (10). With the pulse energies we used, the rates of change were up to 50 pF/s and magnitudes peaked near 10% of the cell's resting membrane capacitance. Effects were reversible upon heat dissipation through the bathing solution. HEK cells expressing prestin showed additional effects on the Boltzmann characteristics of voltage sensor-related NLC. With 20 ms IR pulse durations, V_h was shifted in the positive direction at an average rate of 2.3 V/s, corresponding to 20 mV/°C, and subsequently returned to prior conditions as the heat dissipated. In two cells, delivery of near-maximum laser power produced V_h shift rates of 13–14 V/s. The rates of recovery of linear C_m and V_h with cooling were indistinguishable,

indicating that each is directly coupled to thermal energy. A simple kinetic model of prestin (15) that possesses temperature-sensitive, voltage-dependent transitions that move prestin into the expanded state can mimic our biophysical observations. Thus, we conclude that temperature-induced alteration of transition rates between voltage-dependent conformations of prestin can alter NLC as fast as thermal influences on the membrane double layer (10).

Capacitance

It is well established that capacitance is temperature sensitive; for example, Taylor (22) reported that squid axon capacitance increased 1% per degree centigrade. Others have reported that the kinetics of voltage-dependent channels is temperature sensitive, consequently influencing gating currents (23,24) and necessarily altering their equivalent voltage-dependent capacitance. It is therefore not surprising that prestin NLC is temperature dependent, as we previously showed with slow alterations in bath temperature (3,4). Prestin's NLC V_h shifts ~20 mV per 10°C. What may appear surprising is that prestin can redistribute between expanded and contracted states so rapidly upon IR stimulation, showing V_h shift rates up to 14 V/s. Of course, by nature, prestin is poised to transition between states at kilohertz rates, and apparently is capable of rapidly responding to a variety of energy forms, including mechanical, electrical, and thermal forms (7,8,25,26). Nevertheless, our observations are not simply related to the ability of prestin to rapidly transition between states; more importantly, they reflect the efficacy of realigning the protein's operating voltage range by external influences, namely, adjusting the gain of cochlear amplification.

Our modeling of temperature effects on prestin's voltage-dependent backward rate is similar to that employed to understand TRP channel heat sensitivity (27). In this regard, we recently found that prestin is sensitive to capsaicin (28), an agent that mimics heat activation of TRP channels. However, in prestin, the mechanism of action must be different from that of temperature since it causes negative shifts in V_h, pointing toward action on forward rates. Thus, it will be of interest to evaluate the simultaneous effects of capsaicin and temperature on prestin NLC. Of course, other proposed mechanisms in TRP channels that may also contribute to temperature sensing by prestin include allosteric mechanisms (29) and changes in specific heat capacity (30). Nevertheless, the simplest scheme is likely that of temperature-sensitive transition rates as modeled here, which show excellent agreement with the biophysical data. This is not to say that the sensitivities of the other transitions in the model, i.e., those displaying tension and chloride sensitivity, cannot influence the temperature-sensitive, voltage-dependent transition, as it is well known that a voltage-independent transition can affect the characteristics of a linked voltage-dependent one (31–33).

Currents

In this study, we used blockers to reduce ionic conductances so that we could effectively measure capacitance. We identified two components of residual current: one that is fast, coinciding with the duration of laser heating, and one that follows the temperature of the bath as it cooled. This observation is similar to that of Parker (24), who suggested that the fast component represents gating currents of oocyte ion channels. This was suggested because in the absence of the slow component (i.e., at its reversal potential), transient capacitive-like currents were revealed. Although we do expect that sensor charge movement (i.e., gating-like currents) should arise when prestin's V_h suddenly shifts, we find no evidence of transient-like currents near the reversal potential of our slow component, around 0 mV. We should note that when the cell is held at 0 mV, we are interrogating a linear region of C_m, since NLC V_h is very negative. Our laser-induced currents at 0 mV resemble those found by Shapiro et al. (10), and we conclude that they represent currents generated by rapid changes in linear C_m. The second component of current, which reverses near zero, has some nonlinear features of a conductance, G_{metL}, found in OHCs (20,21). Notably, increases in temperature augment the nonlinear current and are not simply leakage currents.

In summary, we find that SLC26a5 (prestin) is remarkably responsive to fast temperature jumps, rapidly moving its operating point along the voltage axis. This susceptibility to thermal perturbations likely arises from the protein's natural ability to follow voltage changes at acoustic frequencies, but it also has implications for manipulation of cochlear amplifier gain control. Thus, we predict that we may be able to drive auditory sensation by stimulating OHCs with a high-frequency gated IR laser, and manipulate cochlear amplification in vivo.

The authors thank Lei Song and Jun-Ping Bai for their technical assistance and discussions. This research was supported by NIH NIDCD grant DC00273 to J.S.S. and an HHHMI Medical Research Fellowship to O.O.

REFERENCES

1. Ashmore, J., P. Avan, …, B. Canlon. 2010. The remarkable cochlear amplifier. *Hear. Res.* 266:1–17.
2. Zheng, J., W. Shen, …, P. Dallos. 2000. Prestin is the motor protein of cochlear outer hair cells. *Nature.* 405:149–155.
3. Meltzer, J., and J. Santos-Sacchi. 2001. Temperature dependence of non-linear capacitance in human embryonic kidney cells transfected with prestin, the outer hair cell motor protein. *Neurosci. Lett.* 313:141–144.
4. Santos-Sacchi, J., and G. Huang. 1998. Temperature dependence of outer hair cell nonlinear capacitance. *Hear. Res.* 116:99–106.
5. Kakehata, S., and J. Santos-Sacchi. 1995. Membrane tension directly shifts voltage dependence of outer hair cell motility and associated gating charge. *Biophys. J.* 68:2190–2197.
6. Iwasa, K. H. 1993. Effect of stress on the membrane capacitance of the auditory outer hair cell. *Biophys. J.* 65:492–498.

7. Gale, J. E., and J. F. Ashmore. 1994. Charge displacement induced by rapid stretch in the basolateral membrane of the guinea-pig outer hair cell. *Proc. Biol. Sci.* 255:243–249.
8. Santos-Sacchi, J., L. Song, and X. T. Li. 2009. Firing up the amplifier: temperature, pressure and voltage jump studies on Ohc motor capacitance. Concepts and challenges in the biophysics of hearing. Proc. Int. Workshop Mechan. Hearing, 10th, Staffordshire, UK. 363–370.
9. Bian, S., B. W. Koo, …, D. S. Navaratnam. 2010. A highly expressing Tet-inducible cell line recapitulates in situ developmental changes in prestin's Boltzmann characteristics and reveals early maturational events. *Am. J. Physiol. Cell Physiol.* 299:C828–C835.
10. Shapiro, M. G., K. Homma, S. Villarreal, C. P. Richter, and F. Bezanilla. 2012. Infrared light excites cells by changing their electrical capacitance. *Nat. Commun.* 3:736.
11. Yao, J., B. Liu, and F. Qin. 2009. Rapid temperature jump by infrared diode laser irradiation for patch-clamp studies. *Biophys. J.* 96:3611–3619.
12. Santos-Sacchi, J. 2004. Determination of cell capacitance using the exact empirical solution of differential Y/partial differential Cm and its phase angle. *Biophys. J.* 87:714–727.
13. Santos-Sacchi, J., S. Kakehata, and S. Takahashi. 1998. Effects of membrane potential on the voltage dependence of motility-related charge in outer hair cells of the guinea-pig. *J. Physiol.* 510:225–235.
14. Santos-Sacchi, J. 1991. Reversible inhibition of voltage-dependent outer hair cell motility and capacitance. *J. Neurosci.* 11:3096–3110.
15. Song, L., and J. Santos-Sacchi. 2013. Disparities in voltage-sensor charge and electromotility imply slow chloride-driven state transitions in the solute carrier SLC26a5. *Proc. Natl. Acad. Sci. USA.* 110:3883–3888.
16. Bian, S. M., B. W. Koo, …, D. Navaratnam. 2011. Evaluating prestin's changing biophysical attributes in development using a Tet-induced cell line. *AIP Conf. Proc.* 1403:143–147.
17. Reference deleted in proof.
18. Kakehata, S., and J. Santos-Sacchi. 1996. Effects of salicylate and lanthanides on outer hair cell motility and associated gating charge. *J. Neurosci.* 16:4881–4889.
19. Tunstall, M. J., J. E. Gale, and J. F. Ashmore. 1995. Action of salicylate on membrane capacitance of outer hair cells from the guinea-pig cochlea. *J. Physiol.* 485:739–752.
20. Santos-Sacchi, J., V. Rybalchenko, …, D. Navaratnam. 2006. On the temperature and tension dependence of the outer hair cell lateral membrane conductance GmetL and its relation to prestin. *Pflugers Arch.* 452:283–289.
21. Rybalchenko, V., and J. Santos-Sacchi. 2003. Cl- flux through a non-selective, stretch-sensitive conductance influences the outer hair cell motor of the guinea-pig. *J. Physiol.* 547:873–891.
22. Taylor, R. E. 1965. Impedance of the squid axon membrane. *J. Cell. Comp. Physiol.* 66:21–25.
23. Collins, C. A., and E. Rojas. 1982. Temperature dependence of the sodium channel gating kinetics in the node of Ranvier. *Q. J. Exp. Physiol.* 67:41–55.
24. Parker, I. 1989. Ionic and charge-displacement currents evoked by temperature jumps in Xenopus oocytes. *Proc. R. Soc. Lond. B Biol. Sci.* 237:379–387.
25. Santos-Sacchi, J. 1992. On the frequency limit and phase of outer hair cell motility: effects of the membrane filter. *J. Neurosci.* 12:1906–1916.
26. Frank, G., W. Hemmert, and A. W. Gummer. 1999. Limiting dynamics of high-frequency electromechanical transduction of outer hair cells. *Proc. Natl. Acad. Sci. USA.* 96:4420–4425.
27. Voets, T., G. Droogmans, …, B. Nilius. 2004. The principle of temperature-dependent gating in cold- and heat-sensitive TRP channels. *Nature.* 430:748–754.
28. Wu, T., L. Song, …, A. L. Nuttall. 2011. Effect of capsaicin on potassium conductance and electromotility of the guinea pig outer hair cell. *Hear. Res.* 272:117–124.
29. Jara-Oseguera, A., and L. D. Islas. 2013. The role of allosteric coupling on thermal activation of thermo-TRP channels. *Biophys. J.* 104:2160–2169.
30. Clapham, D. E., and C. Miller. 2011. A thermodynamic framework for understanding temperature sensing by transient receptor potential (TRP) channels. *Proc. Natl. Acad. Sci. USA.* 108:19492–19497.
31. Lacroix, J. J., A. J. Labro, and F. Bezanilla. 2011. Properties of deactivation gating currents in Shaker channels. *Biophys. J.* 100:L28–L30.
32. Colquhoun, D. 1998. Binding, gating, affinity and efficacy: the interpretation of structure-activity relationships for agonists and of the effects of mutating receptors. *Br. J. Pharmacol.* 125:924–947.
33. Shirokov, R. 2011. What's in gating currents? Going beyond the voltage sensor movement. *Biophys. J.* 101:512–514, discussion 515–516.